(Received 21 February 2026, Accepted 6 May 2026, Scheduled 18 May 2026)

Time-Domain Analysis of Dual Bandpass Negative Group Delay of RLC-Network Based Lumped Passive Topology

Idiris A. Hussein[1], Florent M. T. Anjara[2], Habachi Bilal[3], Robert Wieser[1], Wan Fayu[1], Lagouge Tartibu[4], Marcellin Atemkeng[5], Glauco Fontgalland[6], Sébastien Lalléchère[7], and Blaise Ravelo[1,*]

[1]*Nanjing University of Information Science & Technology (NUIST), Nanjing, China*
[2]*SERDI, Antsiranana 201, Madagascar*
[3]*Laboratory of Innovative Technologies (LTI) UR 3899, University of Picardie Jules Verne (UPJV), Amiens 80000, France*
[4]*Department of Mechanical Engineering at the University of Johannesburg, Johannesburg 2006, South Africa*
[5]*Department of Mathematics, Rhodes University, Grahamstown 6140, South Africa*
[6]*Brenton School of Engineering, University of Mount Union, Alliance, OH 44601, USA*
[7]*Association Française de Science des Systèmes (AFSCET), 33 ter rue d'Estienne d'Orves, Fontenay-aux-Roses 92260, France*

ABSTRACT: An innovative analysis of a negative group delay (NGD) circuit exhibiting a dual-bandpass (BP) characteristic is presented. The passive BP-NGD topology consists, essentially, of parallel RLC resonant networks. The BP-NGD topology is characterized by the NGD value, NGD center frequency, and attenuation, as functions of the constituent RLC resonant networks. The dual BP-NGD topology is designed using series impedances, which are composed of two distinct parallel RLC networks. After considering the reduced-order model of the passive cell within the NGD frequency range, which enables the determination of component values for the dual BP-NGD circuit, the circuit is formulated as a function of the desired NGD values and center frequencies. The feasibility of the design theory is verified through a proof-of-concept (PoC), designed to operate with the following specifications (1 MHz, −20 µs, −8 dB) and (2 MHz, −20 µs, −8 dB). First, a frequency-domain analysis of the PoC demonstrates the dual BP-NGD behavior, exhibiting an attenuation of approximately 8 dB. Subsequently, time-domain analyses were conducted using input signals with amplitude modulation on sinusoidal carriers at frequencies of 1 MHz, 1.5 MHz, and 2 MHz. The obtained results highlight the possibility of generating output signal envelopes that exhibit a temporal advancement relative to the input ones, provided that the input signal spectrum falls within the NGD bandwidth. However, the output envelope exhibits a positive delay when the input signal spectrum lies outside the NGD frequency band. A potential application principle for the dual BP-NGD circuit is discussed, specifically for the compensation of delay dispersion in electronic and communication systems.

1. INTRODUCTION

Currently, the Negative Group Delay (NGD) function [1–8] constitutes one of the most intriguing electronic circuits; yet it remains relatively unexplored compared to classical circuits, such as filters, amplifiers, oscillators, antennas, converters, and rectifiers, among others, due to its counterintuitive behavior. The benefits of NGD circuit engineering could be significantly enhanced if the theoretical design methodology were to become familiar to most non-specialist engineers. The present study provides a deeper understanding of the design methodology for electronic circuits that operate with the characteristic dual-band (BP) NGD frequency property.

1.1. Potential Applications of the NGD Function

Various studies reveal the ability of the NGD function to enhance performances in electronic engineering [1–10]. This intriguing function demonstrates practical utility for the enhancement of electronic engineering applications, such as in oscillator compensation [1]. At low frequencies (LFs), in the kilohertz (kHz) range, NGD circuits have been employed in medical applications for the detection of physiological signals [2], imparting a predictive effect [3] induced by temporal advancement. The capability of the NGD function to anticipate medical signals [4] can be leveraged in areas such as retinal analysis [5]. Several experimental applications of NGD have been proposed at high frequencies (HFs), including the design of antenna arrays to enhance beamforming precision [6], low-delay ultrasonic transducers [7], the augmentation of amplifier gain-bandwidth [8], and delay reduction in transceiver (Rx-Tx) communication systems [9]. The NGD circuit enables improved signal integrity through the recovery of distorted signals [10]. Before starting the study presented in this research contribution, the following subsections outline the state of the art, thereby highlighting, with greater clarity, existing works concerning the unfamiliar NGD electronic function.

1.2. Physicist Curious Finding on the NGD Phenomenon

The concept of the NGD phenomenon had its roots in fundamental studies related to wave propagation and theory of linear time-invariant (LTI) systems [11, 12]. Specifically, this extraordinary physical phenomenon centered on the characteristics of dispersive media in which group- and phase-velocity

* Corresponding author: Blaise Ravelo (blaise.ravelo@yahoo.fr).

differ from one another [13, 14]. Theoretical studies gained momentum in the mid-20th century, stemming from attempts to understand anomalous dispersion phenomena in optical and electromagnetic media [11, 12]. It has been theoretically demonstrated that the group velocity of a wave packet, when traversing a medium exhibiting anomalous dispersion, can be negative [15]. This counterintuitive concept stems from the dispersive behavior of systems in which the phase varies more rapidly as a function of frequency, a characteristic typically associated with media exhibiting anomalous dispersion [13–15]. The propagation of signals through dispersive media has been demonstrated, with group velocities attaining counterintuitive values within specific frequency domains. Although the term "negative delay" may suggest something nonsensical, NGD phenomena remain consistent with physical principles [16, 17]. The effects of NGD relate to certain phase aspects of superluminal signals that vary over time, rather than transmitting information at a speed exceeding that of light [18]. Indeed, it has been emphasized that the NGD phenomenon does not violate causality [16, 17]. The interaction between input signals was formalized through delay relations, which constitute a fundamental element in LTI systems. It was observed that the output signal of an NGD structure may appear to lead the input one having frequency band where the phase slope is positive. Thus, the concept of the NGD phenomenon was theoretically proposed by physicists [13–15]. Subsequently, advances in the study of the NGD phenomenon attracted the attention of researchers in the field of electronic engineering [19–32].

1.3. Meaning of NGD Phenomenon in Electronic Engineering

Research into the theory, design, and experimentation of electronic circuits featuring NGD has gained momentum. Indeed, the NGD phenomenon was initially studied, starting in the 1990s, using electronic circuits operating across a wide frequency range on the order of kHz [15, 16], megahertz (MHz) and gigahertz (GHz) [17, 18]. Within the scope of circuit theory, it has been established that the NGD effect describes a situation in which the group delays (GD), i.e., the rate of change of a system's phase response with respect to the frequency, assumes a negative value [16, 17, 19, 20]. Consequently, time-domain analysis of the response of NGD circuits indicates that the peak of an output signal can be detected prior to the peak of the corresponding input pulse signal [16, 17, 21, 22]. Technically speaking, an NGD circuit makes it possible to shape the phase slope of the voltage transfer function (VTF) in order to generate a known temporal advancement in the signal [16, 17, 21, 22]. The NGD electronic function has also been the subject of experimentation involving complex baseband audio signals [23]. Various electronic circuit topologies have been proposed [24–28]. For example, the NGD function is typically realized through feedback or feedforward networks [29–31].

The NGD circuit topologies were designed and implemented with high-loss electromagnetic (EM) structures and restricted to very narrowband or single frequencies [19, 20]. Despite the potential applications [1, 6–9], these limitations make NGD circuits unsuitable for modern medium to radio frequency (RF) and microwave wideband communication systems. RF and microwave studies were theoretically and experimentally proposed by using different circuit topologies to improve certain characteristics, such as compact size, attenuation, and bandwidth (BW) of NGD characteristics [32–34]. Due to their ability to move signal envelopes forward while preserving the principle of causality. Then, the time-advance signature of the NGD function was experimented with modulated signals [35].

1.4. Types of NGD Function

Despite the available literature regarding the significance, design, and diversity of NGD effects, reviewed in the previous subsection, it remains challenging for many non-specialist electronics engineers to grasp this counterintuitive function. A fundamental theory of the NGD circuit, inspired by the magnitude response of filters, has enabled the classification of all topologies [36]. Various innovative types of electronic functions have been identified, configured as low-pass (LP) [37], high-pass (HP) [38], and bandpass (BP) [39] NGD topologies. The family of LP-NGD topologies [36, 37], is defined by the group delay (GD) response in the low-frequency (LF) spectrum, starting from DC. In contrast, the HP-NGD topology [36, 38] is defined by a GD response that is consistently negative in the high-frequency (HF) spectrum, starting from a lower bound. Furthermore, the BP-NGD topology [36, 39] corresponds to a type of electronic circuit whose GD response exhibits a negative value within a delimited frequency band of the spectrum. Two elementary LP- and HP-topologies can be combined into a comprehensive design framework for the realization of the BP-NGD topology [39].

1.5. Present Research Contribution and Outline of the Paper

Until now, dual-band NGD circuit has not been studied in depth, particularly in the time domain. For this reason, a theoretical foundation is developed for the design of the dual-frequency BP-NGD circuit utilizing parallel RLC networks, with focus on their frequency selectivity characteristics. The topological approach is considered, followed by the derivation of an analytical model capable of describing the relationship among magnitude, phase, and delay. Subsequently, a comprehensive analysis framework is proposed for the developed methodology.

In this context, the present research work investigates the design and analysis of a dual BP-NGD circuit, consisting of RLC resonant networks. The paper is divided into four distinct sections:

- Section 2 highlights the operating principle of the dual BP-NGD function. The preliminary specifications of the ideal dual-passband NGD responses are defined in the frequency domain. Next, it will be explained why an electronic circuit topology consisting of a passive RLC network cell is capable of operating as a dual-passband NGD function.
- Section 3 focuses on the design theory of the developed dual BP-NGD topology, involving the determination of

formulas that enable the calculation of its constituent components: resistors, inductors, and capacitors.
- Section 4 analyzes the responses of a proof-of-concept (PoC) representing a dual passive BP-NGD circuit, comparing the AC responses or frequency responses at different BWs, obtained from the analytical calculations based on an established model and from simulations.
- Section 5 examines the innovative time-domain analysis of the PoC responses of the dual BP-NGD circuit. Transient input signals modulating three different sine carriers, both within and outside the NGD BW, are considered.
- Section 6 explains the potential application of the dual BP-NGD circuit.
- Section 7 is the final conclusion of the paper.

2. OPERATION PRINCIPLE OF DUAL BP-NGD FUNCTION

The present section describes the dual BP-NGD functionality in the frequency domain.

2.1. Preliminary Definition of BP-NGD Function

The fundamental analysis of the present dual BP-NGD circuit is based on the consideration of its VTF represented in the frequency domain. Theoretical modelling necessitates the consideration of a black-box two-port system as represented in Fig. 1.

FIGURE 1. Black box two-port system.

By denoting the Laplace variable defined as $s = j2\pi f$ with frequency f, the theoretical exploration of the VTF is using the input voltage and the output voltage, $V_{in}(s)$ and $V_{out}(s)$, respectively. The VTF associated with the system shown in Fig. 1 is defined as follows:

$$T(s) = \frac{V_{out}(s)}{V_{in}(s)}. \tag{1}$$

The frequency domain analysis is explored via the transmittance:

$$T(j2\pi f) = \Re e[T(j2\pi f)] + j\Im m[T(j2\pi f)]. \tag{2}$$

The VTF associated magnitude and phase are expressed by, respectively:

$$\begin{aligned} T(f) &= |T(j2\pi f)| \\ &= \sqrt{\{\Re e[T(j2\pi f)]\}^2 + \{\Im m[T(j2\pi f)]\}^2} \end{aligned} \tag{3}$$

$$\varphi(f) = a\tan\left[\frac{\Im m[T(j2\pi f)]}{\Re e[T(j2\pi f)]}\right]. \tag{4}$$

The key parameter of BP-NGD analysis is the GD defined by:

$$GD(f) = \frac{-1}{2\pi}\cdot\frac{\partial\varphi(f)}{\partial f} \tag{5}$$

with $\varphi(f)$ expressed in radians. The recalled analytical definitions enable the development of the building block of the electronic circuit NGD analysis, as explored in the next subsection.

2.2. Specifications of BP-NGD Frequency Response

The BP-NGD analysis is based on considering the ideal responses of GD and magnitude diagrams in the frequency domain, as shown in Fig. 2(a) and in Fig. 2(b), respectively.

The main specifications of the BP-NGD function are:

- The NGD cut-off frequencies f_{n1} and $f_{n2}(f_{n2} > f_{n1})$ are defined by:

$$\begin{cases} GD(f_{n1}) = 0 \\ GD(f_{n2}) = 0 \end{cases} \tag{6}$$

- The NGD center frequency $f_n \in [f_{n1}, f_{n2}]$ is defined by:

$$GD(f) = GD(f_n) = GD_n < 0 \tag{7}$$

- The NGD BW is defined by:

$$\Delta f_n = f_{n2} - f_{n1} \tag{8}$$

- The VTF magnitude at the NGD center frequency is defined by:

$$T_n = T(f_n) \tag{9}$$

These specifications will be used to characterize the dual BP-NGD frequency response in the following subsection.

2.3. Typical Frequency Response and Equivalent Reduced Model of Dual BP-NGD Circuit

A dual BP-NGD circuit is proposed, as shown in Fig. 3. It is composed of two resonant parallel RLC-networks $R_1L_1C_1$ and $R_2L_2C_2$, which are connected in series and a shunt resistor R_a at the output.

The ideal frequency responses illustrating the design methodology enable the identification of the equivalent circuits of the dual BP-NGD function as highlighted in Fig. 4. In particular, Fig. 4(a) depicts the ideal diagram of the GD response, which is specified by two NGD center frequencies denoted f_1 and f_2 associated with NGD BWs Δf_1 and Δf_2, respectively.

The associated NGD values of the dual BP-NGD circuit within NGD BWs are $GD_1 = GD(f_1) < 0$ and $GD_2 = GD(f_2) < 0$, respectively. The ideal magnitude diagram of the dual BP-NGD function specified by the magnitudes around center frequencies f_1 and f_2 denoted by $T_1 = T(f_1)$ and $T_2 = T(f_2)$ is proposed in Fig. 4(b), respectively. After the topological identification, a generalized theory associating an RLC-network-based cell enables the identification of the equivalent circuit reduced model of our dual BP-NGD circuit represented by BP-NGD$_1$ and BP-NGD$_2$ cells, as shown in Figs. 4(c) and 4(d), respectively. The magnitude, phase and GD frequency responses of the dual band circuit postulated as equivalent to BP-NGD$_1$ and BP-NGD$_2$ in the vicinity of NGD center frequencies f_1 and f_2, respectively, will be formulated in the next section.

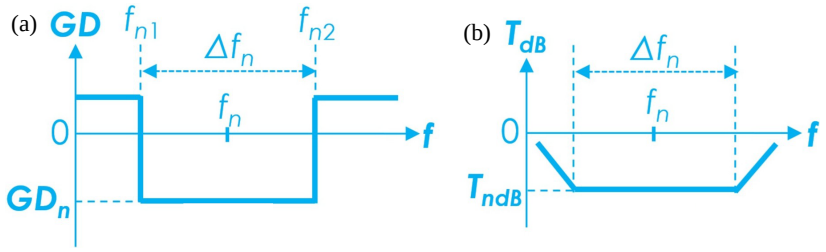

FIGURE 2. (a) GD and (b) magnitude diagrams illustrating the BP-NGD ideal response.

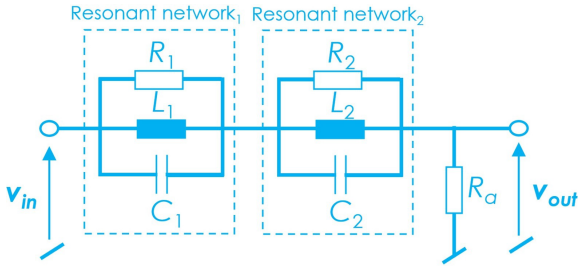

FIGURE 3. Dual BP-NGD circuit understudy.

3. DESIGN THEORY OF DUAL BP-NGD PASSIVE TOPOLOGY CONSTITUTED BY PARALLEL RLC-RESONANT NETWORKS

In this section, the theory of passive topology is described, which exhibits the dual BP-NGD effect. The theoretical approach is established from the VTF defined in Equation (1) and the BP-NGD specification preliminarily defined in Subsection 2.2.

3.1. Analytical Description of BP-NGD Circuit within the Single Operation Band

The passive topology proposed in Fig. 5 represents the elementary cell constituting the dual BP-NGD circuit to be developed in the present study.

This circuit consists of a parallel impedance $R_nL_nC_n$ mounted in series and shunted at the output by a resistor R_a. Based on (1), the VTF is expressed as follows:

$$T(s) = \frac{R_a\left(R_nL_nC_ns^2 + L_n\,s + R_n\right)}{R_aR_nL_nC_ns^2 + L_n\left(R_a + R_n\right)s + R_nR_a} \tag{10}$$

According to (3) and (4), the magnitude and phase of the previous VTF are given by:

$$T(f) = \frac{R_a\sqrt{R_n^2[1-(2\pi f)^2L_nC_n]^2 + (2\pi f)^2L_n^2}}{\sqrt{R_a^2R_n^2[1-(2\pi f)^2L_nC_n]^2 + (2\pi f)^2L_n^2(R_a+R_n)^2}} \tag{11}$$

$$\varphi(f) = a\tan\left\{\frac{2\pi fL_n}{R_n\left[1-(2\pi f)^2L_nC_n\right]}\right\} - a\tan\left\{\frac{2\pi fL_n(R_a+R_n)}{R_nR_a\left[1-(2\pi f)^2L_nC_n\right]}\right\} \tag{12}$$

The corresponding GD obtained by using (5) is expressed as:

$$GD(f) = \frac{\begin{array}{l}R_n^2L_n\left[1+(2\pi f)^2L_nC_n\right]\left[R_a^2R_n^2-(2\pi f)^2L_n\right.\\ \left.\left[L_n(R_a+R_n)+2R_aR_n^2C_n\right]+(2\pi f)^4\right.\\ \left.R_aR_n^2L_n^2C_n^2\right]\end{array}}{\begin{array}{l}\left[R_n^2+(2\pi f)^2L_n(L_n-2R_n^2C_n)+(2\pi f)^4\right.\\ \left.R_n^2L_n^2C_n^2\right]\left[R_n^2R_a^2+(2\pi f)^2L_n\right.\\ \left.\left[R_a^2(L_n-2R_n^2C_n)+(2R_a+R_n)R_nL_n\right]\right.\\ \left.+(2\pi f)^4R_a^2R_n^2L_n^2C_n^2\right]\end{array}} \tag{13}$$

The NGD center frequency is regarded as the parallel impedance $R_nL_nC_n$ resonance frequency, which is expressed as:

$$f_n = \frac{1}{2\pi\sqrt{L_nC_n}} \tag{14}$$

At this center frequency, the BP-NGD circuit magnitude proposed in Equation (9) is given by:

$$T_n = \frac{R_a}{R_a+R_n} \tag{15}$$

Furthermore, the GD at the NGD center frequency expressed in Equation (7) becomes:

$$GD_n = \frac{-2R_n^2C_n}{R_a+R_n} < 0 \tag{16}$$

Previous GD was unconditionally negative for any component parameters of the passive cell, as shown in Fig. 5. The NGD cut-off frequencies are pedagogically derived as the root of Equation (6) or simply of the GD numerator:

$$f^4 - \frac{L_n(R_a+R_n)+2R_aR_n^2C_n}{4\pi^2R_aR_n^2L_nC_n^2}f^2 + \frac{R_a}{16\pi^4L_n^2C_n^2} = 0 \tag{17}$$

It implies obviously the following cut-off frequencies:

$$f_{n1} = \frac{\sqrt{2C_n + \frac{L_n(R_a+R_n)}{R_n^2R_a} - \sqrt{\left[2C_n + \frac{L_n(R_a+R_n)}{R_n^2R_a}\right]^2 - 4C_n^2}}}{2\pi\sqrt{2}C_n\sqrt{L_n}} \tag{18}$$

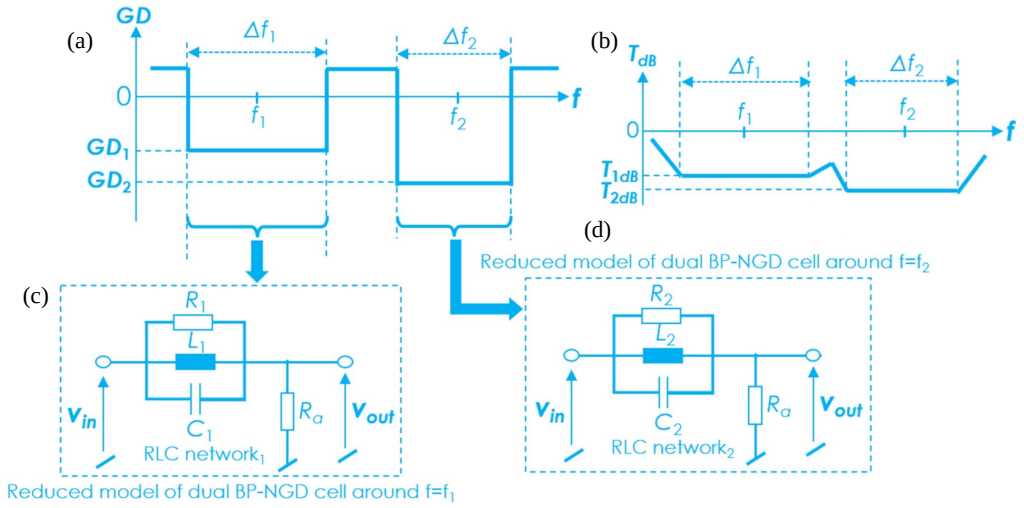

FIGURE 4. Design methodology with dual BP-NGD (a) GD and (b) magnitude diagram. (c) BP-NGD$_1$ and (d) BP-NGD$_2$ reduced equivalent circuit model to dual BP-NGD topology shown in Fig. 3 with the NGD frequency bands in proximity of f_1 and f_2, respectively.

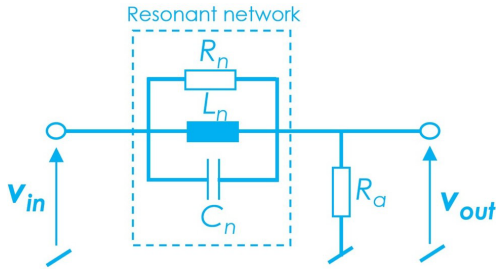

FIGURE 5. Basic topology of BP-NGD passive cell.

$$f_{n2} = \frac{\sqrt{2C_n + \frac{L_n(R_a+R_n)}{R_n^2 R_a} + \sqrt{\left[2C_n + \frac{L_n(R_a+R_n)}{R_n^2 R_a}\right]^2 - 4C_n^2}}}{2\pi\sqrt{2}C_n\sqrt{L_n}} \tag{19}$$

Therefore, the NGD BW can be written as:

$$\Delta f_n = \frac{\sqrt{2C_n + \frac{L_n(R_a+R_n)}{R_n^2 R_a} + \sqrt{\left[2C_n + \frac{L_n(R_a+R_n)}{R_n^2 R_a}\right]^2 - 4C_n^2}} - \sqrt{2C_n + \frac{L_n(R_a+R_n)}{R_n^2 R_a} - \sqrt{\left[2C_n + \frac{L_n(R_a+R_n)}{R_n^2 R_a}\right]^2 - 4C_n^2}}}{2\pi\sqrt{2}C_n\sqrt{L_n}} \tag{20}$$

Moreover, we can remark that:

$$f_{n1} f_{n2} = f_n^2 \tag{21}$$

Based on the magnitude and NGD analytical expressions, design formulas for the resistors, inductors, and capacitors constituting the dual BP-NGD circuit are established in the following subsection.

3.2. Design Equations for Dual BP-NGD Circuit

The proposed design equations determine the parameters R_1, L_1, C_1, R_2, L_2, C_2, and R_a of the circuit topology illustrated in Fig. 3. Thus, the design depends on the choice of:

- NGD center frequencies f_1 and f_2,
- NGD values $t_1 = GD_1 < 0$ and $t_2 = GD_2 < 0$,
- And attenuations T_1 and T_2.

By fixing output resistor R_a, the RLC components can be determined as follows:

- The values of resistors R_1 and R_2 are obtained by substituting $R_n = R_1$ and $R_n = R_2$ in Equation (15). Therefore, we have:

$$R_1 = \left(\frac{1-T_1}{T_1}\right) R_a \tag{22}$$

$$R_2 = \left(\frac{1-T_2}{T_2}\right) R_a \tag{23}$$

- The capacitors can be calculated by inverting Equation (16):

$$C_1 = \frac{-T_1 t_1}{2(1-T_1)^2 R_a} \tag{24}$$

$$C_2 = \frac{-T_2 t_2}{2\,(1-T_2)^2 R_a} \tag{25}$$

- And the inductors extracted from Equation (14) are given by:

$$L_1 = \frac{1}{4\pi^2 f_1^2 C_1} \tag{26}$$

$$L_2 = \frac{1}{4\pi^2 f_2^2 C_2} \tag{27}$$

The following subsection describes the design methodology of the dual-BP-NGD circuit using the previously established design equations.

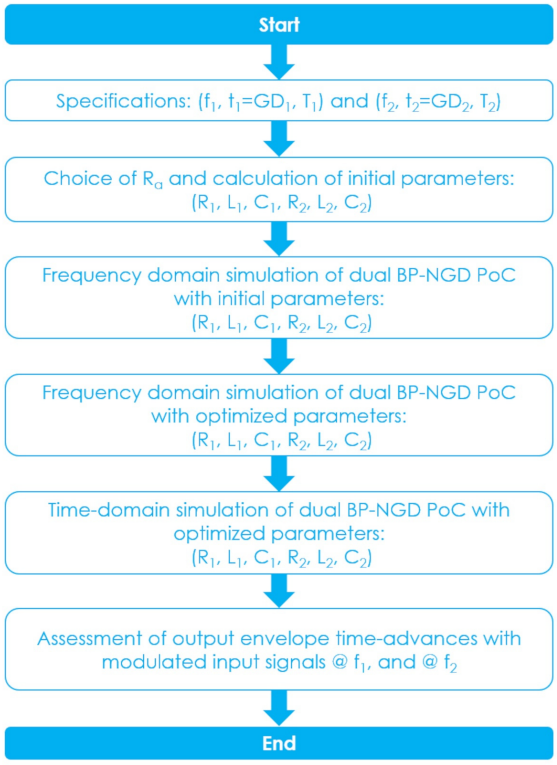

FIGURE 6. Flowchart of design methodology illustrating the dual BP-NGD circuit study.

3.3. Design Methodology of Dual BP-NGD Circuit

The flowchart viewed in Fig. 6 indicates the BP-NGD circuit design methodology, including six successive steps. The main tasks suggested during the design of the dual BP-NGD circuit PoC can be described as follows:

- Step 1: This initial step involves specifying the NGD center frequencies (f_1, f_2), time-advances ($GD_1 < 0$, $GD_2 < 0$) and attenuation (T_1, T_2).
- Step 2: This step is the choice of resistor R_a. The ideal values of resistors, inductors, and capacitors (R_1, R_2, L_1, L_2, C_1, C_2) constituting the resonant impedances of the dual BP-NGD circuit, shown in Fig. 3, can be calculated using Equations (22), (23), (24), (25), (26), and (27).
- Step 3: This step consists in calculating the frequency responses of dual BP-NGD BP-NGD_1 and BP-NGD_2 circuit VTFs. Thereafter, the specifications are introduced in Step 1 and analytically verified.
- Step 4: In this step, the frequency domain modelling and/or simulation of the dual BP-NGD circuit representing the PoC can be performed in the SPICE environment using optimized values of (R_1, R_2, L_1, L_2, C_1, C_2) by fixing the load R_a. After the PoC, the magnitude, phase, and GD frequency responses of the dual BP-NGD circuit PoC are compared with those of BP-NGD_1 and BP-NGD_2 in this step.
- Step 5: This original step of the design focuses on time-domain analysis to confirm the feasibility of dual BP-NGD behavior with the optimized circuit PoC.
- Step 6: The feasibility of the dual BP-NGD circuit is finalized in this step by assessing the time-advance signature performed from the PoC output signals modulating f_1 and f_2 sine carrier input signals.

Following the established design methodology indicated by the flowchart in Fig. 6, a PoC was designed using a familiar tool, and the results of the feasibility study are discussed in the next section.

4. DESIGN AND FREQUENCY DOMAIN SIMULATION ANALYSES OF DUAL BP-NGD CIRCUIT PROOF-OF-CONCEPT

In the present section, a clear numerical example of a dual BP-NGD circuit is presented with respect to arbitrarily defined specifications based on frequency domain analyses. The obtained results validating the BP-NGD aspect of MATLAB calculation responses of PoC VTF model will be compared with LTSPICE simulation ones.

4.1. Description of the Dual BP-NGD Circuit PoC

To design the dual BP-NGD PoC, we have considered the arbitrarily chosen specifications of NGD center frequency, NGD value, and attenuation in the two-frequency BWs of interest, denoted by BW_1 and BW_2 addressed in Table 1.

TABLE 1. Specifications of BP-NGD_1 and BP-NGD_2 networks constituting the dual BP-NGD PoC shown in Fig. 3.

Function	Name	Value
BP-NGD_1	f_1	1 MHz
	$t_1 = GD(f_1)$	-20 µs
	$T(f_1)$	-8 dB
BP-NGD_2	f_2	2 MHz
	$t_2 = GD(f_2)$	-20 µs
	$T(f_2)$	-8 dB

The PoC was designed in the LTSPICE environment after the application of the design methodology developed in Subsection 3.3. By using the design Equations (22) and (23) for resistors, Equations (24) and (25) for inductors, and Equations (26) and (27) for capacitors, the ideal values of constituent component parameters of the PoC circuit can be obtained, as listed in Table 2.

TABLE 2. List of components constituting the dual BP-NGD PoC shown in Fig. 6(b).

Nature	Name	Ideal value	Nominal value
Resistor	R_1	1512 Ω	15 kΩ
	R_2	1512 Ω	15 kΩ
	R_a	1 kΩ	1 kΩ
Inductor	L_1	230.5 µH	240 µH
	L_2	57.3 µH	56 µH
Capacitor	C_1	10.99 nF	11 nF
	C_2	10.99 nF	11 nF

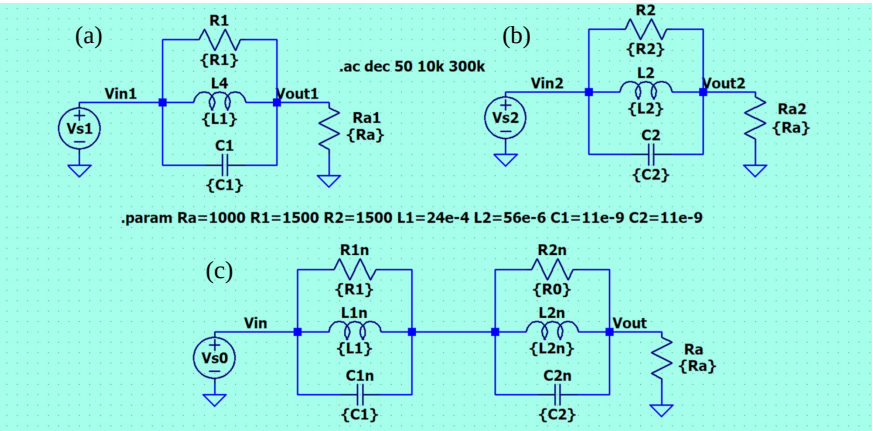

FIGURE 7. Schematic of (a) BP-NGD$_1$, (b) BP-NGD$_2$ and (c) BP-NGD circuit PoC designed in the LTSPICE environment.

Subsequently, the PoC circuit was designed after slight optimization of the ideal resistor, inductor, and capacitor components. Fig. 7 presents the schematics of BP-NGD$_1$, BP-NGD$_2$, and the dual BP-NGD circuit schematized in the LTSPICE environment. During the simulation, the constituent components were replaced with their nominal values from the E24 series, which corresponds to a 5% tolerance. The frequency domain analysis of the dual BP-NGD circuit schematics depicted in Fig. 7 was performed in the frequency range defined as $f_{\min} = 10\,\text{kHz}$ and $f_{\max} = 300\,\text{kHz}$. The simulation of the PoC enabled validation of the previously established VTF modelling approach for the dual BP-NGD topology in Section 3.

The presented feasibility study is elaborated by comparing the AC results specified in Subsection 2.3. The frequency domain results obtained from our PoC using the dual BP-NGD BP-NGD$_1$ and BP-NGD$_2$ single cell circuits are analyzed in the following subsections.

4.2. Magnitude Frequency Responses of the Dual BP-NGD PoC

Figure 8 shows the magnitude frequency responses of the dual BP-NGD circuit PoC shown in Fig. 7 compared with the single BP-NGD cells BP-NGD$_1$ and BP-NGD$_2$, which are plotted as the red and blue curves, respectively. The theoretical magnitude calculated with MATLAB of the PoC is represented by "Dual BP-NGD$_{\text{model}}$" and the LTSPICE tool simulation ones are labelled "Dual BP-NGD$_{\text{simulation}}$". These plots compare the modeled and simulated magnitudes of BP-NGD$_1$ (plotted in the red solid curve), BP-NGD$_2$ (plotted in sky-blue solid curve), modelled dual BP-NGD circuit (plotted in green dot curve), and the simulated dual BP-NGD PoC (plotted in black dashed curve). As seen in Fig. 8(a), a good agreement between the considered circuit modelling and simulation of the dual BP-NGD circuit PoC was obtained from $f_{\min}$ to $f_{\max}$. Moreover, the magnitudes of the BP-NGD responses of the dual and single circuits fit well, as witnessed by Fig. 8(b) in the first frequency band [60 kHz, 140 kHz]. Subsequently, a similar agreement between the calculation and simulations is obtained in the second frequency band as depicted in Fig. 8(c) within the interval [160 kHz, 240 kHz].

4.3. GD Analysis of Dual BP-NGD PoC

The fundamental characteristics of the dual BP-NGD function rely on the GD response. Therefore, we studied the effectiveness of the developed design method of the dual BP-NGD topology by comparing the PoC of single cell, namely, BP-NGD$_1$ and BP-NGD$_2$. Before the examination of GD responses, we considered the phase responses of BP-NGD$_1$, BP-NGD$_2$, and the modelled and simulated dual BP-NGD circuits displayed in Fig. 9(a) in the working frequency band [$f_{\min}$, $f_{\max}$]. One finds that:

- As seen in Fig. 9(b) within [60 kHz, 140 kHz], the phase response of BP-NGD$_1$ cell is well correlated to the dual BP-NGD circuit PoC one in the first NGD frequency band in proximity of $f = f_1$.
- However, the phase response of BP-NGD$_2$ cell within [160 kHz, 240 kHz] viewed in Fig. 9(c) highlights a phase shift of approximately $\pi/3$ rad at $f = f_2$. Despite the phase shift, the typical behavior of BP-NGD response is observed in the vicinity of f_2.

In continuation of the phase response comparison, the GD responses of dual BP-NGD circuit PoC versus the BP-NGD$_1$ and BP-NGD$_2$ cell ones were also determined and analyzed.

As a result of the comparative study, the confirmation of the design method through the equivalent BP-NGD cells is illustrated by GD responses in the working frequency band [$f_{\min}$, $f_{\max}$], plotted in Fig. 10(a). The validation of the reduced equivalent model is upheld by the occurrence of the following responses:

- As seen in Fig. 10(b), the GD of the dual BP-NGD PoC is corroborated by the reduced equivalent cell BP-NGD$_1$ cell after a closer look at the frequency band [60 kHz, 140 kHz], which includes the proximity of $f = f_1$. Subsequently, the BP-NGD$_2$ cell GD plotted with a blue solid line is almost zero.
- The reverse situation is found within [160 kHz, 240 kHz] as shown in Fig. 10(c), where the BP-NGD$_1$ cell GD is almost zero. Moreover, the GD response of BP-NGD$_2$ cell is well correlated to the dual BP-NGD circuit PoC one.

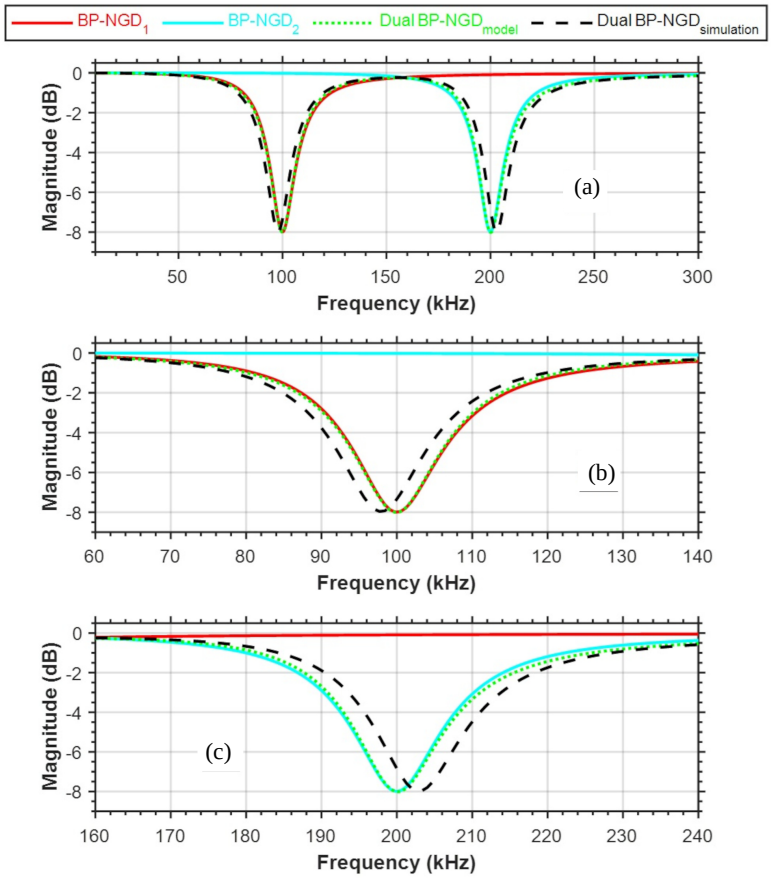

FIGURE 8. Comparison of magnitudes of the dual BP-NGD circuit schematic shown in Fig. 7: (a) whole working frequency band [$f_{\min}$, $f_{\max}$], and zoomed in frequency bands, (b) [60 kHz, 140 kHz] and (c) [160 kHz, 240 kHz].

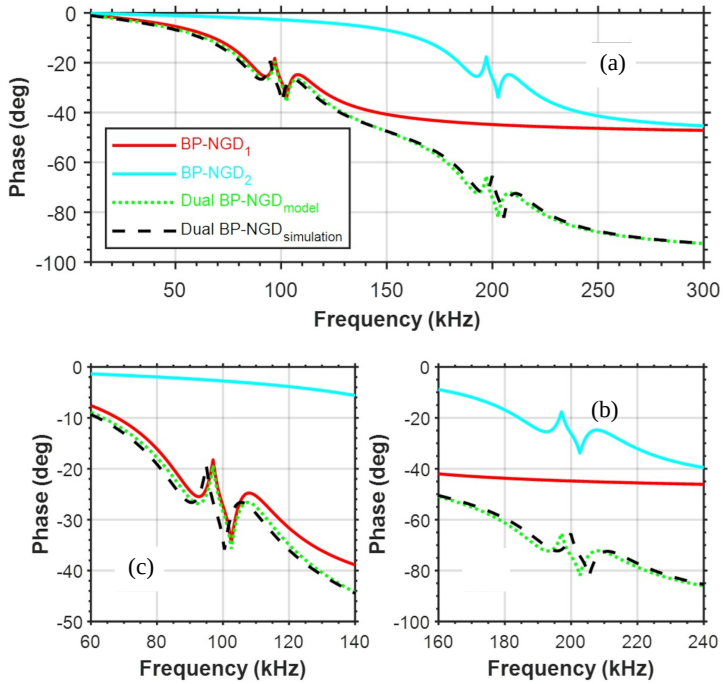

FIGURE 9. Phase responses of the dual BP-NGD circuit schematic shown in Fig. 7: (a) whole frequency band [10 kHz, 300 kHz], and zoomed in frequency bands, (b) [60 kHz, 140 kHz] and (c) [160 kHz, 240 kHz].

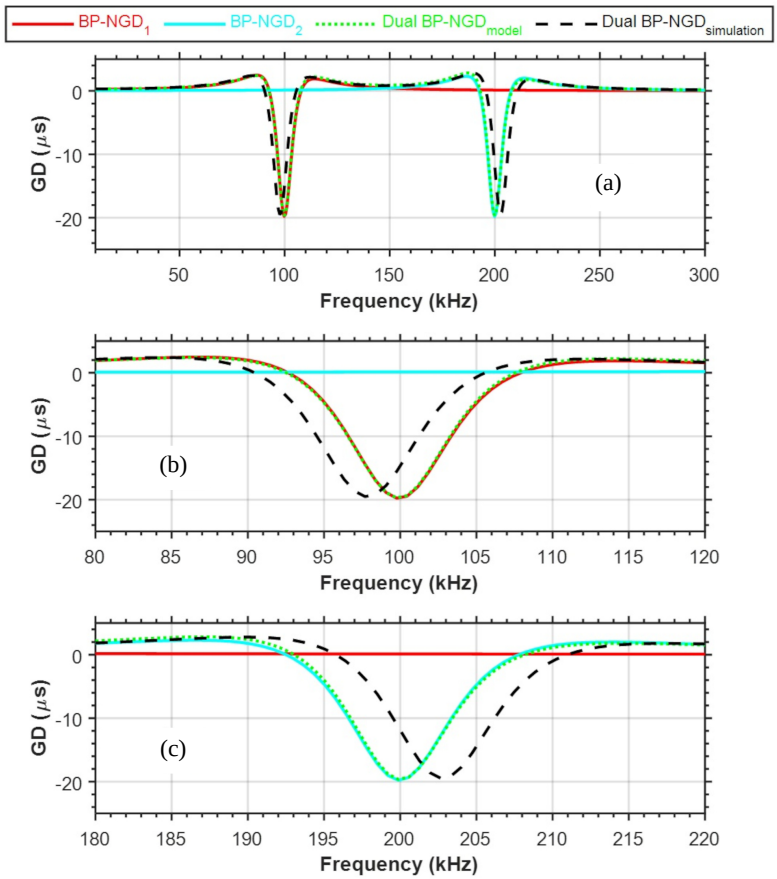

FIGURE 10. Comparison of GDs of the dual BP-NGD circuit schematic shown in Fig. 7: (a) whole frequency band [10 kHz, 300 kHz], and zoomed in frequency bands, (b) [60 kHz, 140 kHz] and (c) [160 kHz, 240 kHz].

TABLE 3. BP-NGD characteristics of modelled single cell BP-NGD$_1$, BP-NGD$_2$, dual BP-NGD PoC versus simulated BP-NGD PoC shown in Fig. 7.

Considered circuit	NGD center frequency $f = f_n$	NGD BW Δf_n	Magnitude @ $f = f_n$	$GD(f_n)$
Modeled dual BP-NGD PoC @ f_1	99.8 kHz	49.7 kHz	-8.003 dB	-19.7 µs
Simulated dual BP-NGD PoC @ f_1	97.7 kHz	50.4 kHz	-7.96 dB	-19.5 µs
BP-NGD$_1$	99.8 kHz	49.7 kHz	7.99 dB	-19.76 dB
Modeled dual BP-NGD PoC @ f_2	200.6 kHz	49.6 kHz	-8.003 dB	-19.6 µs
Simulated dual BP-NGD PoC @ f_2	203.3 kHz	49.9 kHz	-7.95 dB	-19.46 µs
BP-NGD$_2$	200.6 kHz	49.6 kHz	-7.95 dB	-19.78 µs

A brief synthesis of the overall BP-NGD responses, including the dual-band BP-NGD and the reduced equivalent cell NGD center frequency shift, is discussed in the next subsection.

4.4. Synthetic Recapitulative Dual BP-NGD Results of PoC

The relevance of the design method of the dual BP-NGD modelling was assessed by comparing the synthetic specifications from the calculated and simulated dual BP-NGD PoC with those from the single-cell BP-NGD$_1$ and BP-NGD$_2$. The comparison results highlight the excellent agreement between the reduced equivalent circuit model and the simulated dual BP-NGD circuit PoC summarized in Table 3.

In brief, the dual BP-NGD specifications of our PoC from the MATLAB calculation and LTSPICE simulation are well correlated and can be recapitulated as follows:

- The obtained NGD center frequencies f_1 and f_2, and the targeted frequencies specified in Table 1 are achieved with an accuracy of less than 2%.

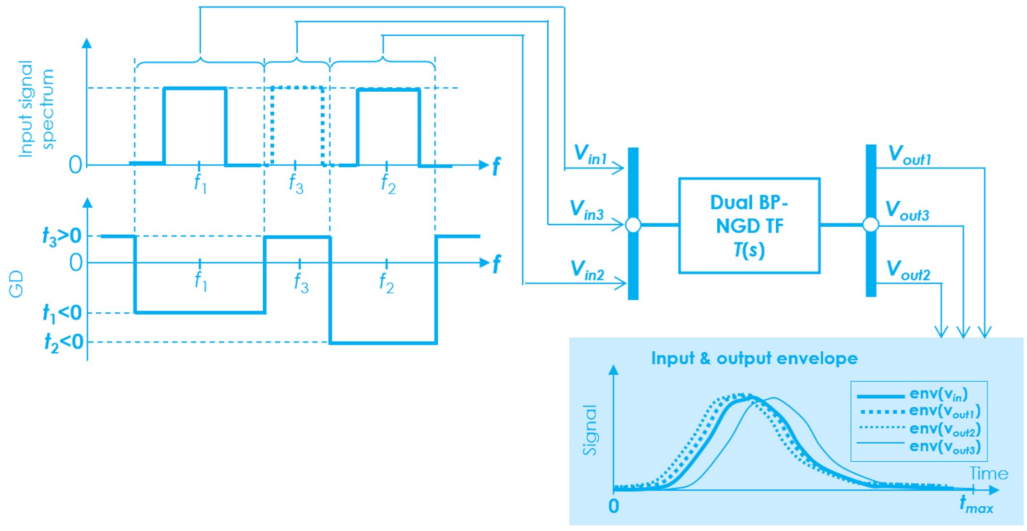

FIGURE 11. Illustration diagram of dual BP-NGD circuit analysis in the time domain.

- The good correlation of the NGD BW with the NGD cut-off frequencies is addressed in the 3rd column of comparison Table 3.
- The single- and dual-BP-NGD cell attenuations at the NGD center frequency present a difference of less than 0.1 dB.
- And more importantly, NGD values $GD_{n=1,2} = GD(f = f_{n=1,2})$ are very accurate.

Further understanding of the usefulness of the dual BP-NGD function is based on time-domain analyses as discussed in the following section.

5. TIME DOMAIN ANALYSES

In this section, the time-domain interpretation of the dual BP-NGD behavior of the PoC, which was previously analyzed in the frequency domain, is innovatively analyzed.

5.1. Process of the Time Domain Analysis of Dual BP-NGD Circuit Response

The present analyses aim to verify, in an innovative time-domain manner, the response of dual BP-NGD PoC. In other words, the feasibility study is carried out with the transient simulation responses of the PoC presented in Fig. 7. Doing this, the three-input voltage signals denoted v_{in1}, v_{in2} and v_{in3} with amplitude max $(v_{in,k=\{1,2,3\}}) = 1\,\text{V}$ modulating sine carriers having different frequencies $f_1 = 100\,\text{kHz}$, $f_2 = 200\,\text{kHz}$ and $f_3 = 150\,\text{kHz}$ were considered. These three frequencies were chosen after spectral analysis of GD responses, displayed in Fig. 10 with respect to the dual BP-NGD condition in Equation (28).

$$\begin{cases} GD(f_1) = t_1 < 0 \\ GD(f_2) = t_2 < 0 \\ GD(f_3) = t_3 > 0 \end{cases} \tag{28}$$

The transient simulation duration was fixed at $t_{\max} = 0.72\,\text{ms}$. The analysis consists of assessing the delay between the input envelope $v_{in,k=\{1,2,3\}} = v_{in}(f_k)$ and the PoC output $v_{out,k} = \{1, 2, 3\}$.

Figure 11 highlights the operating principle of the proposed time-domain analysis by showing the relationship among f_k, GD t_k, and the delays between output envelopes env$(v_{in,k=\{1,2,3\}})$ and env$(v_{out,k=\{1,2,3\}})$. The following subsections treat the obtained time-domain results.

5.2. Time-Domain Response with Input v_{in1} Modulating Sine Carrier Frequency $f = f_1$

Figure 12 plots the LTSPICE transient response v_{out1} of the dual BP-NGD circuit PoC with the input signal v_{in1}.

From the obtained transient result, we can underline that:

- In this study case, v_{in1} was modulating sine carrier frequency f_1. As shown in Fig. 12(a), v_{in1} has a bi-exponential waveform with rise-time about 130 µs and fall-time about 500 µs.
- A good correlation coefficient can be observed between v_{in1} and v_{out1} where $\max(v_{out1}) \approx 426\,\text{mV}$ as seen in Fig. 12(b). As predicted by the frequency-domain response of the PoC TF plotted in Fig. 8(b) @ $f = f_1$, output attenuation can be assessed. For the time-domain simulation, the peak ratio is $\max(v_{out1})/\max(v_{in1}) \approx -7.38\,\text{dB}$.
- Despite the attenuation, the normalized plots of Fig. 12(c) showing the absolute values of input and output envelopes env(v_{in1}) (blue curve) and env(v_{out1}) (navy curve) over the time interval $[0, t_{\max}]$ present a pulse signal peak time-advance of approximately $t_{n1} \approx -24.8\,\mu\text{s} < 0$.
- A closer look at the zoomed-in plots of v_{in1} and v_{out1} within the time intervals [0, 150 µs] and [200 µs, 300 µs] represented in Figs. 12(d) and 12(e) further confirms the envelope advances of the output signal envelope rise- and fall-fronts, respectively.

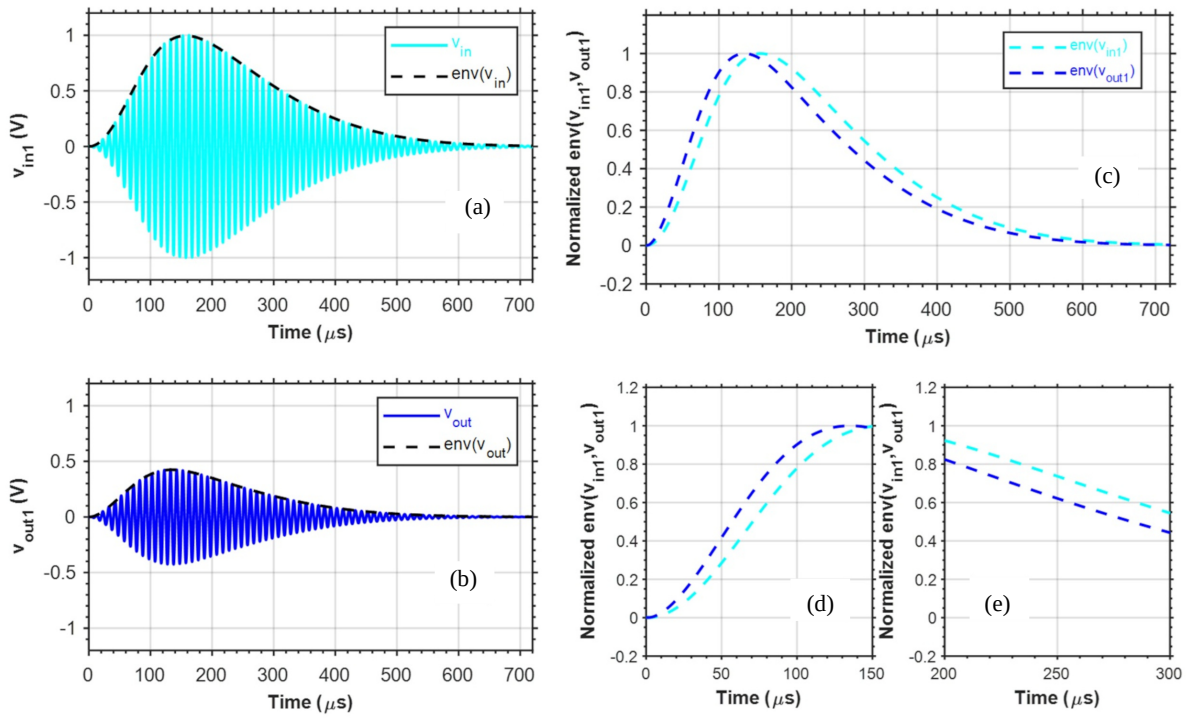

FIGURE 12. Transient response of dual BP-NGD PoC showing plot of (a) v_{in1}, (b) v_{out1} and (c) env(v_{in1}) vs env(v_{out1}) over time interval $[0, t_{\max}]$. The zoom in plots on time intervals (d) [0, 150 µs] and (e) [200 µs, 300 µs].

- The obtained transient response of v_{in1} confirms the BP-NGD time-domain signature with NGD center frequency $f = f_1$ with signal envelope in the time-advance.

To strengthen the dual BP-NGD feasibility study, further time-domain analysis with input modulating carrier frequency $f = f_2$ is conducted in the next subsection.

5.3. Time-Domain Response with Input v_{in2} Modulating Sine Carrier Frequency $f = f_2$

Similar to the previous case study, the present time-domain analysis is based on input signal v_{in2} modulating a carrier at the second NGD center frequency $f = f_2$. The obtained transient results emphasize the following points:

- One can observe that input v_{in2} plotted in Fig. 13(a) has the same envelope as previous input v_{in1}.
- The output peak shown in Fig. 13(b) is $\max(v_{in2}) \approx 432\,\text{mV}$. This corresponds to the results of the transient time-domain simulation with attenuation represented by the peak ratio $\max(v_{out2})/\max(v_{in2}) \approx -7.27\,\text{dB}$. Once again, the time-domain results explain the frequency domain response in the second BP-NGD frequency band.
- The normalized plots of v_{in2} and v_{out2} displayed in Fig. 13(c) enable the understanding of the time-advance signature owing to the BP-NGD function. We evaluate the peak time advance as $t_{n2} \approx -19.3\,\mu\text{s} < 0$.
- Similar to the previous subsection, the advances of the output envelope rise- and fall-fronts are witnessed by the zoomed-in plots in Figs. 13(d) and 13(e), respectively.

In addition to the study performed around the NGD center frequencies $f = f_1$ and $f = f_2$, the PoC time-domain response outside the NGD band with the input modulating carrier frequency $f = f_3$ is discussed in the next subsection.

5.4. Time-Domain Response with Input v_{in3} Modulating Sine Carrier Frequency $f = f_3$

In this last case of study, the focus is on the transient response of v_{in3} obtained from the same input envelope as in the two previous cases. Consequently, one remarks from the obtained results that:

- One recalls that, as earlier introduced in Subsection 5.1, v_{in3} plotted in Fig. 14(a) corresponds to the signal spectrum out of the NGD band, where the delay is expected to be positive.
- The PoC response v_{out3} plotted in Fig. 14(b) has peak maximum of about $\max(v_{out3}) \approx 0.98\,\text{V}$. This corresponds to the PoC with a low attenuation $\max(v_{out3})/\max(v_{in3}) \approx -0.14\,\text{dB}$.
- Nevertheless, as expected by the dual BP-NGD theory, a comparison of the transient signals v_{in3} and v_{out3} displayed in Fig. 14(c) in the time interval $[0, t_{\max}]$.
- The transient results are clarified by the zoomed-in rise- and fall-fronts in Fig. 14(d) and Fig. 14(e), respectively, enabling the understanding of the disappearance of the NGD signature. In other words, we assessed the positive delay effect between the peaks of env(v_{in3}) and env(v_{out3}) of about $t_{n3} \approx 0.84\,\mu\text{s} > 0$.

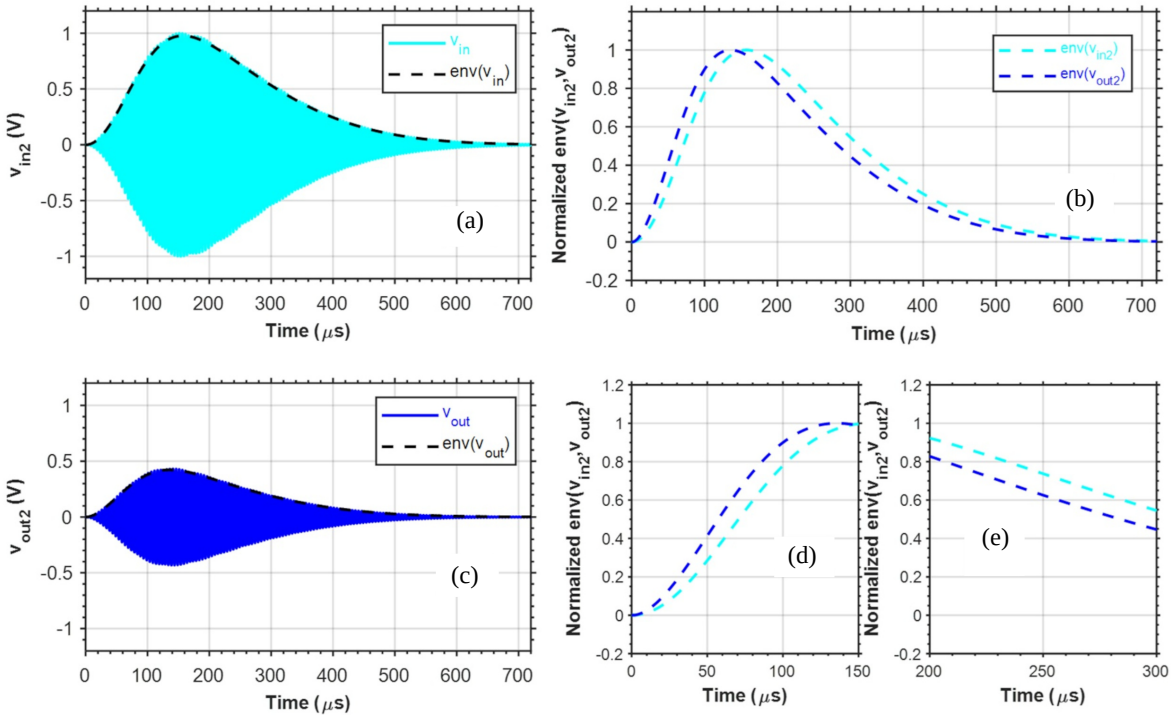

FIGURE 13. Transient response of dual BP-NGD PoC showing plot of (a) v_{in2}, (b) v_{out2} and (c) env(v_{in2}) vs env(v_{out2}) over the time interval $[0, t_{\max}]$. The zoom in plots on time intervals (d) [0, 150 µs] and (e) [200 µs, 300 µs].

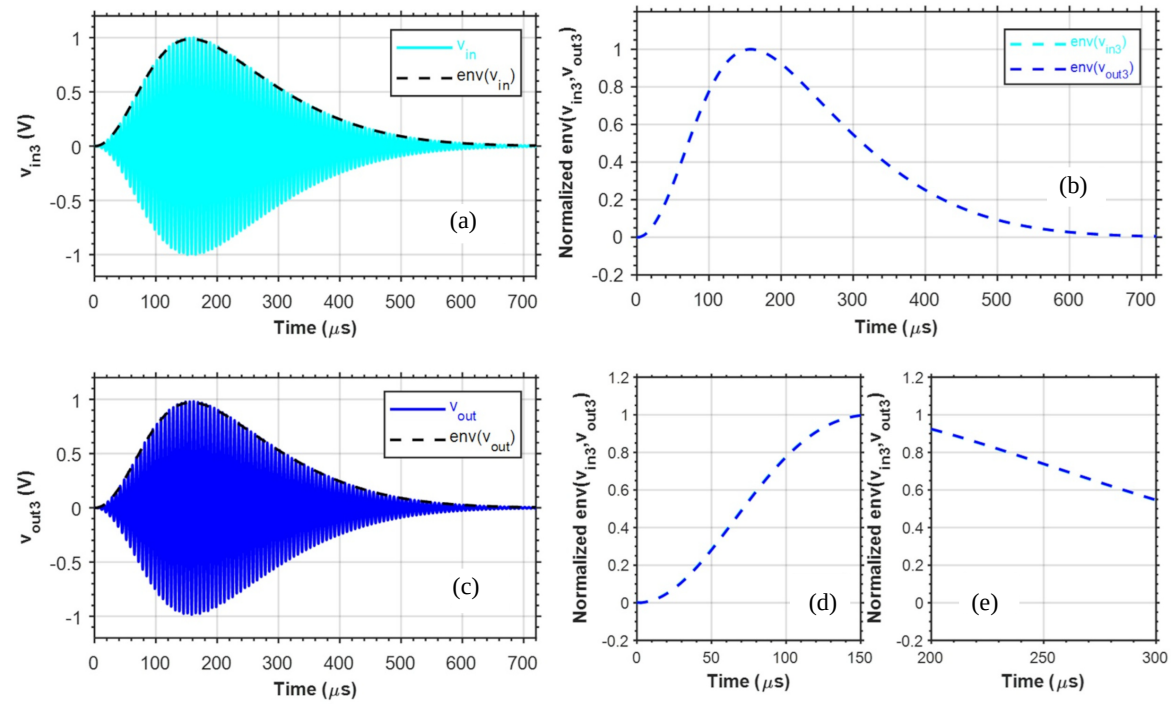

FIGURE 14. Transient response of dual BP-NGD PoC showing plot of (a) v_{in3}, (b) v_{out3} and (c) env(v_{in3}) vs env(v_{out3}) over the time interval $[0, t_{\max}]$. The zoom in plots on time intervals (d) [0, 150 µs] and (e) [200 µs, 300 µs].

After the time-domain feasibility study, an ideal case of dual BP-NGD circuit application is proposed in the following section.

6. DISCUSSION ON DUAL BP-NGD CIRCUIT APPLICATION

The dual BP-NGD circuit can be used to compensate for delay dispersion in electronic systems. The principle of compensat-

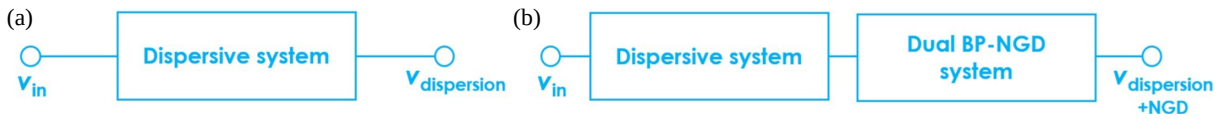

FIGURE 15. Synoptic diagram of (a) dispersion, (b) dual BP-NGD and dispersion + dual BP-NGD system.

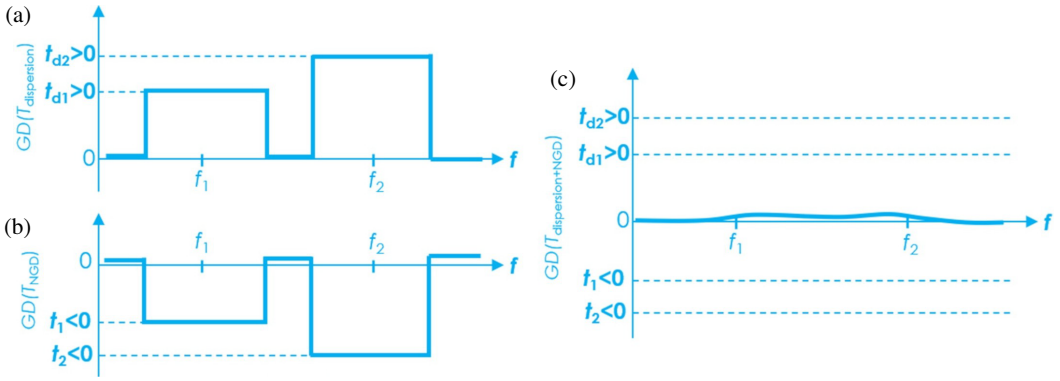

FIGURE 16. GD ideal responses of (a) dispersion, (b) dual BP-NGD and (c) dispersion + dual BP-NGD system.

ing for delay dispersion is discussed in the following subsections.

6.1. Dispersive and Dual BP-NGD System Description

To illustrate the potential applications, the synoptic diagram representation is considered. The overall system has an input voltage denoted as v_{in}. As illustrated in Fig. 15(a), the dispersive system is assumed to operate with output voltage $v_{dispersion}$. The TF associated with the dispersive system is named $T_{dispersion}(f)$.

A systemic solution against dispersion involves, for example, downstream (or upstream) cascading the dispersive system with a dual BP-NGD system as shown in Fig. 15(b). The NGD TF is termed $T_{NGD}(f)$. The corresponding output voltage of the overall system is denoted $v_{dispersion+NGD}$. The overall or total system TF is termed $T_{dispersion+NGD}(f)$. The GD frequency responses are analyzed in the next subsection.

6.2. GD Responses Illustrating the Dual BP-NGD Application to Compensate Delay Dispersion

Based on the GD definition proposed earlier in Equation (4), we can highlight the expected frequency response illustrating the dual BP-NGD circuit application. The typical delay dispersion is by dual band delays around two frequencies f_1 and f_2. Fig. 16 displays the ideal behavior of each GD.

The operation principle of dispersion can be obtained with the GD response described as follows:

- As shown in Fig. 16(a), the delay dispersion can be formulated using the frequency response expressed as $t_{d1} = GD[T_{dispersion}(f_1)] > 0$ and $t_{d2} = GD[T_{dispersion}(f_2)] > 0$.
- The dual BP-NGD system must be designed with respect to the dispersion system response. Accordingly, we can take the NGD specifications as $t_1 = GD[T_{NGD}(f_1)] < 0$ and $t_2 = GD[T_{NGD}(f_2)] < 0$. Therefore, we have a typical GD diagram presented in Fig. 16(b).
- The compensation analytically means the total GD becomes close to zero. To do this, we have the total GD at the central frequnecies f_1 and f_2 given by: $GD[T_{dispersion+NGD}(f_1)] = GD[T_{dispersion}(f_1)] + GD[T_{NGD}(f_1)] \approx 0$ and $GD[T_{dispersion+NGD}(f_2)] = GD[T_{dispersion}(f_2)] + GD[T_{NGD}(f_2)] \approx 0$.

6.3. Time-Domain Response Illustrating Dual BP-NGD Circuit Application

To better comprehend the delay dispersion compensation method, the typical waveform of input voltage v_{in} assumed as a pulse signal with envelope env(v_{in}) is shown in Fig. 17.

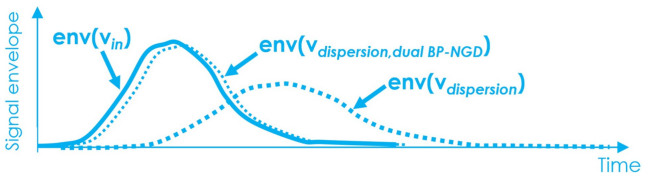

FIGURE 17. Time-domain responses of dispersion, dual BP-NGD and dispersion + dual BP-NGD system.

Owing to the delay dispersion, the dispersion system transient response denoted by env$(v_{dispersion})$ can be significantly spread along time, as illustrated in Fig. 17. Because of the NGD compensation, the overall system output should behave similarly to env$(v_{dispersion,dual\ BP\text{-}NGD})$. This technique of delay compensation with a dual or multi-band BP-NGD circuit enables:

- To reduce the signal delay in the electrical and electronic systems.
- To reduce the multi-resonance effect in the communication or digital system.

- To improve the signal integrity degraded by the sensor system imperfection.
- And to avoid the communication system electromagnetic interference (EMI).

7. CONCLUSION

An innovative study of a dual BP NGD-type passive circuit in both the frequency and time domains is developed. The meaning of the dual BP-NGD function is defined using frequency ideal responses. The main topology of the dual BP-NGD consists of R, L, and C resonant passive circuits. Owing to the VTF analysis, it was found that the value of its GD around the RLC-network resonance frequency, which is assumed as the NGD center frequency, is always negative for any values of the cell. Furthermore, design formulas and a methodology for designing the dual BP-NGD circuit are established.

The feasibility of the dual BP-NGD design method was confirmed by simulations of an arbitrarily chosen circuit PoC analyzed in both the frequency and time domains. Therefore, a strong correlation was observed between the frequency domain simulation results from the dual BP-NGD PoC and the equivalent single BP-NGD operating around the NGD center frequency. The modeled and simulated GD responses verified the calculated specifications, including the attenuation, NGD center frequency coinciding with RLC-resonant frequencies, NGD BWs, and NGD values.

Furthermore, the simulation results highlighted the expected dual BP-NGD function with the possibility to propagate modulated pulse signals in time advance. The dual BP-NGD behavior was confirmed by the comparison of time advances of the input and output envelope peaks. In addition, it was noted that outside the NGD band, the output envelope presents a positive delay because of the disappearance of the NGD effect.

The potential application of the dual BP-NGD system is discussed. The dual BP-NGD circuit can collectively improve signal integrity and reduce undesirable EMI in electronic and electrical systems.

As future work, we have the following work plan:

- Research on multi-band NGD topologies that can be used with electronically tunable circuits is ongoing.
- Prototyping and time-domain experimental validation of theoretical predictions through simulation, thereby advancing the practical implementation of the dual BP-NGD circuit is currently in progress.
- The integration of a dual BP-NGD integrated circuit in modern communication systems is planned by expecting improvements in signal processing systems.

ACKNOWLEDGEMENT

This research work is supported by the National Natural Science Foundation of China (NSFC) research program under Grant No. 62371241.

REFERENCES

[1] Broomfield, C. D. and J. K. A. Everard, "Broadband negative group delay networks for compensation of microwave oscillators and filters," *Electronics Letters*, Vol. 36, No. 23, 1931–1933, 2000.

[2] Hymel, C. M., M. H. Skolnick, R. A. Stubbers, and M. E. Brandt, "Temporally advanced signal detection: A review of the technology and potential applications," *IEEE Circuits and Systems Magazine*, Vol. 11, No. 3, 10–25, 2011.

[3] Voss, H. U., "A universal negative group delay filter for the prediction of band-limited signals," *arXiv preprint arXiv:1706.07326*, Jun. 2017.

[4] Baloglu, O., O. Cicekoglu, and N. Herencsar, "Single CFOA-based active Negative Group Delay circuits for signal anticipation," *Engineering Science and Technology, an International Journal*, Vol. 48, 101590, 2023.

[5] Chou, P.-Y., J.-F. Chien, K. S. Chen, Y.-T. Huang, C.-C. Chen, and C. K. Chan, "Anticipation and negative group delay in a retina," *Physical Review E*, Vol. 103, No. 2, L020401, 2021.

[6] Oh, S.-S. and L. Shafai, "Compensated circuit with characteristics of lossless double negative materials and its application to array antennas," *IET Microwaves, Antennas & Propagation*, Vol. 1, No. 1, 29–38, 2007.

[7] Choi, H., "Development of negative-group-delay circuit for high-frequency ultrasonic transducer applications," *Sensors and Actuators A: Physical*, Vol. 299, 111616, Nov. 2019.

[8] Choi, H., Y. Jeong, C. D. Kim, and J. S. Kenney, "Bandwidth enhancement of an analog feedback amplifier by employing a negative group delay circuit," *Progress In Electromagnetics Research*, Vol. 105, 253–272, 2010.

[9] Ravelo, B., H. Du, D. Kholodnyak, X. Jin, and F. Wan, "Tx-Rx communication delay compensation by using negative group delay circuits," *IEEE Transactions on Instrumentation and Measurement*, Vol. 74, 1–11, 2025.

[10] Zhang, Y., X. Su, R. Wieser, R. S. Galan, and B. Ravelo, "Reshaping of distorted signal with low-pass type negative group delay RL-network circuit," *Circuits, Systems, and Signal Processing*, Vol. 44, No. 4, 2308–2329, 2025.

[11] Sommerfeld, A., *Lectures on Theoretical Physics: Optics*, Academic Press, New York, 1954.

[12] Brillouin, L., *Wave Propagation and Group Velocity*, Academic Press, New York, NY, USA, 1960.

[13] Chu, S. and S. Wong, "Linear pulse propagation in an absorbing medium," *Physical Review Letters*, Vol. 48, No. 11, 738, 1982.

[14] Segard, B. and B. Macke, "Observation of negative velocity pulse propagation," *Physics Letters A*, Vol. 109, No. 5, 213–216, 1985.

[15] Garrett, C. G. B. and D. E. McCumber, "Propagation of a Gaussian light pulse through an anomalous dispersion medium," *Physical Review A*, Vol. 1, No. 2, 305, 1970.

[16] Mitchell, M. W. and R. Y. Chiao, "Causality and negative group delays in a simple bandpass amplifier," *American Journal of Physics*, Vol. 66, No. 1, 14–19, 1998.

[17] Mitchell, M. W. and R. Y. Chiao, "Negative group delay and "fronts" in a causal system: An experiment with very low frequency bandpass amplifiers," *Physics Letters A*, Vol. 230, No. 3–4, 133–138, Jun. 1997.

[18] Cao, H., A. Dogariu, and L. J. Wang, "Negative group delay and pulse compression in superluminal pulse propagation," *IEEE Journal of Selected Topics in Quantum Electronics*, Vol. 9, No. 1, 52–58, Jan.–Feb. 2003.

[19] Lucyszyn, S., I. D. Robertson, and A. H. Aghvami, "Negative group delay synthesiser," *Electronics Letters*, Vol. 29, No. 9, 798–800, 1993.

[20] Lucyszyn, S. and I. D. Robertson, "Analog reflection topology building blocks for adaptive microwave signal processing applications," *IEEE Transactions on Microwave Theory and Techniques*, Vol. 43, No. 3, 601–611, 1995.

[21] Nakanishi, T., K. Sugiyama, and M. Kitano, "Demonstration of negative group delays in a simple electronic circuit," *American Journal of Physics*, Vol. 70, No. 11, 1117–1121, 2002.

[22] Kitano, M., T. Nakanishi, and K. Sugiyama, "Negative group delay and superluminal propagation: An electronic circuit approach," *IEEE Journal of Selected Topics in Quantum Electronics*, Vol. 9, No. 1, 43–51, 2003.

[23] Munday, J. N. and R. H. Henderson, "Superluminal time advance of a complex audio signal," *Applied Physics Letters*, Vol. 85, No. 3, 503–505, Jul. 2004.

[24] Nako, J., C. Psychalinos, A. S. Elwakil, and B. J. Maundy, "Power-law negative group delay filters," *Electronics*, Vol. 13, No. 3, 522, 2024.

[25] Nako, J., C. Psychalinos, B. J. Maundy, and A. S. Elwakil, "Elementary negative group delay filter functions," *Circuits, Systems, and Signal Processing*, Vol. 43, No. 6, 3396–3409, 2024.

[26] Maundy, B. J., A. S. Elwakil, and C. Psychalinos, "Systematic design of negative group delay circuits," *AEU — International Journal of Electronics and Communications*, Vol. 174, 155060, Jan. 2024.

[27] Banchuin, R., "On the fractional domain analysis of negative group delay circuits," *International Journal of Circuit Theory and Applications*, Vol. 52, No. 3, 1531–1546, 2024.

[28] Nako, J., C. Psychalinos, A. S. Elwakil, and B. J. Maundy, "A note on the bandwidth of negative group delay filters," *International Journal of Circuit Theory and Applications*, Vol. 53, No. 1, 477–484, Jan. 2025.

[29] Abuelma'atti, M. T. and Z. J. Khalifa, "A new CFOA-based negative group delay cascadable circuit," *Analog Integrated Circuits and Signal Processing*, Vol. 95, No. 2, 351–355, 2018.

[30] Voss, H. U. and N. Stepp, "A negative group delay model for feedback-delayed manual tracking performance," *Journal of Computational Neuroscience*, Vol. 41, No. 3, 295–304, 2016.

[31] Voss, H. U., "A delayed-feedback filter with negative group delay," *Chaos: An Interdisciplinary Journal of Nonlinear Science*, Vol. 28, No. 11, 113113, Nov. 2018.

[32] Chaudhary, G., J. Jeong, Q. Wang, and Y. Jeong, "A design of source-degenerated CMOS active negative group delay circuit using bonding wire," *IEICE Electronics Express*, Vol. 16, No. 7, 20190010, 2019.

[33] Chaudhary, G., J. Jeong, P. Kim, and Y. Jeong, "Negative group delay circuit with improved signal attenuation and multiple pole characteristics," *Journal of Electromagnetic Engineering and Science*, Vol. 15, No. 2, 76–81, Apr. 2015.

[34] Meng, Y., P. Li, A. Yuan, and Z. Lan, "Compact broadband negative group delay circuit with flatness and bandwidth enhancement," *Electronics*, Vol. 13, No. 15, 3056, 2024.

[35] Siddiqui, O. F., S. J. Erickson, G. V. Eleftheriades, and M. Mojahedi, "Time-domain measurement of negative group delay in negative-refractive-index transmission-line metamaterials," *IEEE Transactions on Microwave Theory and Techniques*, Vol. 52, No. 5, 1449–1454, 2004.

[36] Ravelo, B., "Similitude between the NGD function and filter gain behaviours," *International Journal of Circuit Theory and Applications*, Vol. 42, No. 10, 1016–1032, Oct. 2014.

[37] Shi, J., J. Cui, H. E. Silochi, R. Wieser, R. S. Galan, N. M. Murad, and B. Ravelo, "Positive-to-negative tunable delay circuit designed with NGD RC network," *International Journal of Circuit Theory and Applications*, Vol. 52, No. 10, 5010–5024, Oct. 2024.

[38] Fenni, S., F. Haddad, A. Jaomiary, S. S. Yazdani, F. E. Sahoa, L. Ramifidisoa, M. Guerin, W. Rahajandraibe, and B. Ravelo, "Investigation on four-port mono-capacitor circuit with high-pass negative group delay behavior," *International Journal of Circuit Theory and Applications*, Vol. 50, No. 2, 478–495, Feb. 2022.

[39] Boussougou, Y. C. M., E. J. R. Sambatra, A. Jaomiary, L. Ramifidisoa, N. M. Murad, J.-P. Kouadio, S. Ngoho, F. E. Sahoa, S. Baccar, and R. Randriatsiferana, "Bandpass-type NGD design engineering and uncertainty analysis of RLC-series resonator based passive cell," *Progress In Electromagnetics Research C*, Vol. 121, 65–82, 2022.